Chapter XX

ANALYSIS OF HYDROGEN BEHAVIOR IN HIGH STRENGTH STEELS JOINTS WELDED BY SMAW

G. A. Mansilla* , M. N. Inés and M.N. Delpupo

Metallurgy Department/ Development and Materials Technology Center (DEYTEMA), Facultad Regional San Nicolás. Universidad Tecnológica Nacional, San Nicolás de los Arroyos, Buenos Aires, Argentina

ABSTRACT

Nowadays, the worldwide consumption of welded steel products continues growing, as they are vital for the automotive, construction and machinery industries, among others. There is extensive research and development regarding hydrogen embrittlement (HE), mainly devoted to hydrogen assisted cracking. Major sources of hydrogen (H) in a weld come from water/moisture chemically bonded to electrodes, apart from the hydrogen contained in the chemical composition of steel and the environmental hydrogen absorbed by the liquid pool generated by electric arcs. During cooling, part of this H may diffuse from the welded joints into the heat affected zone (HAZ) and base metal (BM) or remain occluded in irreversible traps, such as interfaces inclusions-matrix, precipitates and martensite needles. However, H can also be trapped in vacancies and dislocations. Literature refers to this as reversible or diffusible H, that is, traps where H has a short residence time at temperature of interest and, thus, is responsible for failure. In general, the greater the amount of H retained, the greater the risk of cracking and embrittlement, leading to a significant variation in the mechanical properties of the welded steel joint. Owing to this, it is extremely important to study steel susceptibility to H damage and its consequent embrittlement.

The first part of this chapter is related to the interactions between H in high strength steels during welding processes, emphasizing the effects on the mechanical properties of these welded joints. Then, H electrolytic charge in two high strength steels (SAE 1045 and a hot rolled microalloyed steel with vanadium, titanium and niobium – MLC) and experimental methodology are detailed. Afterwards, the mechanical behavior of hydrogenated steels joints and electron microscopy techniques employed are evaluated. Finally, there is a discussion of the obtained results and the conclusions reached.

*Corresponding Author Email: gmansilla@frsn.utn.edu.ar.

Keywords: hydrogen, welding, high strength steels, mechanical behavior.

1. INTRODUCTION

Hydrogen (H) entry into metals leads to a variety of processes that may cause premature failure. The high mobility of H atoms is influenced by its smaller size, in comparison to iron atoms, which allows to enter easily to metals crystalline lattice, preferably in interstitial sites.

Hydrogen embrittlement (HE) has been studied for years because of its important consequences for the industry, not only for the harmful effects on materials, (Bertolino 2012) but also due to its negative economic impact on subsequent processing stages. It is well known that atomic or molecular hydrogen that enters steel may be anchored in low energy "reversible traps" (grain boundaries, dislocations, elastic stress fields), and in those of greater energy refereed to as “irreversible” (interfaces with inclusions, precipitates, etc.). Hydrogen desorption from these latter sites is produced at high temperatures (approximately 600ºC), they are all characterized by having potential energy wells greater than those related to lattice interstitial sites or "reversible sites" (Inés and Mansilla 2012) (Stratmann 2003) (Coudreuse and Charles 1987).

Strong traps reduce steel susceptibility to hydrogen embrittlement, because of the entailing increase of hydrogen saturation content into steel, although this trapped hydrogen is innocuous (Bladeshia 2016). As a trap provides a favorable environment for the hydrogen atom to reside in, there is an energy reduction ΔE following its transfer from a normal to a defect site (Nordlander et al. 1986), so that ΔE is negative. Trapping energies have been widely investigated for all kinds of defects, using experimental techniques such as thermal desorption spectroscopy or mathematical models (Maroef et al. 2002) (Frappart et al. 2011). Delayed fracture occurs when steel submitted to a relatively small stress, with respect to its fracture strength, undergoes spontaneous brittle failure after a period in service. This failure under static low load is attributed to the presence of irreversible hydrogen (Suh 2014), which implies that the trapped hydrogen is not able to diffuse through the lattice and contribute to diffusible hydrogen during service conditions and during the intended service life of the steel – H remains trapped. In thermal desorption experiments, ‘irreversibly’ hydrogen trapped is only released at higher temperatures. At a low temperature, H is weakly trapped. However, the actual temperature at which significant quantities of hydrogen are desorbed also depends on the heating rate (Katano 2001). The most likely sources of H income are working atmospheres, galvanizing and welding procedures, and localized corrosion – which deserves special monitoring on steels – where the concentration of H in metal surface can be very large, constituting quite complex situations of H income (Nelson 1974) (Inés et al. 2013).

The influence of initial hydrogen content was studied by Zafra et al. (2018), who measured pre-charged samples under high temperature hydrogen pressure, increased with decreasing steel tempering temperature because hydrogen microstructural trapping is greater in distorted, high energy martensitic microstructures. They found that embrittlement indexes (strength and

reduction in area) obtained using hydrogen pre-charged notch tensile specimens increase with steel hardness.

In this way, it is well documented that when a sufficient amount of hydrogen is combined with a crack, susceptible microstructure or welding residual stresses possess a greater risk of hydrogen assisted cracking (HAC) (Kumar and Yu-ichi 2013).

Diffusible hydrogen in a heat affected zone (HAZ) has received considerable attention in the existing literature due to its frequency in steel welding (Wildash et al, 1998). Regardless of extensive research and developments, manufacturers still experience HAC regularly, particularly during welding of high strength structural steels (Davidson 1998). HAC is not only limited to welding, it can also occur during steel manufacturing or when in service. There are two deterioration problems associated with the occurrence of HAC. First, the probability of HAC in a welding joint is maximum at temperatures in the range of -50 to 150° C, which also includes ambient temperature (Davis 2006) (Linnert 1965). Second, the HAC of a welding joint is often delayed for hours or even days after welding and, though extensive, cracks can be difficult to detect.

High-strength steels have been widely used in construction of large-scale welded structures. The principal advantage of these steels is good combination of strength and toughness, but also good weldability. Production volumes of advanced high strength steels (AHSS) are growing rapidly due to material and energy savings in several fields. High-strength steels are especially suitable for pipelines, offshore facilities, naval vessels and ships (Pal et al. 2017). In order to use their potential fully, it is necessary to minimize any danger of unexpected failure caused by hydrogen embrittlement (Rudomilova et al. 2018). Quenched and tempered steels are especially thought to be sensitive to hydrogen degradation, which causes a significant limitation of use. The embrittlement effect of H over high strength steels is a topic that has been extensively discussed in the available literature (Hirth 1980) (Kimet al. 2009) (Nagumo 2001) (Novak et al. 2010). Specifically, welding operations, common in industries, constitute one of the main entry routes for H. Cracking is undesirable in a weld because it causes a reduction in the mechanical properties, and thus poses a potential threat.

The problem is due to the absorption of hydrogen from seawater, promoted when cathodic protection is applied to steel to control corrosion. In such situations, hydrogen effect is greater near room temperature and decreases with increasing strain rate. Hydrogen degradation is more pronounced with increasing hydrogen content or charging rate and with increasing steel strength. A number of intense research studies have reported the behavior and effects of hydrogen in steel and its welds (Pandey et al. 2016).

In view of the nature of the environment surrounding the weld fusion zone (Gedeon and Eagar 1990) (Ouden and Griebling 1990) (Banerjee et al. 1993), the quantity of H both in the weld bead and in the HAZ may come from the humidity of the consumable used, from the work atmosphere or from the presence of hydrogenated compounds in the electrodes coating, which decompose when in contact with the electric arc and let hydrogen enter into the welding metal (Pitrun 2004). Furthermore, the degree of H absorption depends on the nature and composition of the welding atmosphere, the temperature distribution on the surface of the liquid sink and the surface area thereof. After being absorbed on the surface, H is transported by convection

and diffusion into the liquid bath (welding metal) and by diffusion into the solid material. As expressed by Alam et al. (1997), as the fusion zone of the weld cools, some hydrogen is desorbed from the weld surface, while diffusion from the weld metal inwards continues in a transient manner (Mundar et al. 1997). The heat generated by the welding arc breaks the hydrogen bonding of the molecules of the surrounding atmosphere, releasing two hydrogen atoms per dissociation; thus, damage in welding is attributed to the absorption of these atoms.

Because hydrogen embrittlement can occur due to spontaneous fissures both in the weld metal and in the HAZ and can lead to catastrophic failure of structures, the way it enters and interacts with steel internal structure is studied. Focus is especially given to the hydrogen trapped in high energy sites where adequate post welding treatments are needed to prevent harmful effects. It is very difficult to detect HAC in weldments because it occurs at room temperature and it appears hours or days after welding completion, even though it may cause catastrophic failure of components while in service (Pandey et al. 2017) (Yue 2014) (Padhy and Komizo 2013). Basically, HE is a loss of mechanical properties caused by the combined effect of H presence in atomic form and stress. The hydrogen gas enters the arc atmosphere and hence, it also enters the solidifying weld region in arc welding process.

A study about grains deformation, (Wasim and Djukic 2019) has described the effect of hydrogen-induced mechanical degradation of low carbon steel at macro-, micro- and nano-levels in the hydrogen-rich acidic environments. Microcracks and blisters formed by the hydrogen penetration found are responsible for the reduction in the strength of low carbon steel. Locally, high hydrogen concentration also favours hydrogen embrittlement, particularly decohesion - HEDE (hydrogen-enhanced decohesion mechanism), intergranular cracking, grain boundaries and grain boundary triple junction.

Following current trends in experimental and modelling approaches, a unified HELP (hydrogen embrittlement localized plasticity) + HEDE model based on specific microstructural mapping of dominant HE mechanisms with implications on fracture process and the resulting hydrogen-assisted fracture modes is extensively treated by Djukic et al. (2019),.

On some occasions, there are welding procedures performed at sea. In this context, water as a welding environment intensifies the action of unfavorable factors that influence the susceptibility of welded steel joints to cold cracking. The increase of the cooling rate contributes to brittle structures in HAZ and to increasing residual stresses values. So, welded structural steel joints made directly in water are characterized by a high susceptibility to cold cracking (Fydrych 2013). Cracks in welds are observed in all test joints made underwater. The phenomenon is consistent with information contained in the literature sources related to tested steels weldability (Tasak 2002). Specimens made in the air were characterized by a much lower susceptibility to crack forming.

Hydrogen induced cracking occurs after weld cooling (hence the term cold cracking) and is often delayed for many hours while atomic hydrogen diffuses to areas of high tensile stress. At microstructural views in a tensile stress field, the hydrogen changes to its molecular form, causing cracking. Cracking may occur in the HAZ or weld metal, and it may be longitudinal or transverse. For carbon steels, cracking is more likely to occur in the HAZ because carbon steel electrodes are usually low in carbon and the weld metal is generally not hardenable. Underbead

cracks in the HAZ lie parallel to the fusion line, they do not normally extend to the surface and may therefore be difficult to detect.

In this chapter, hydrogen effects on Shield Metal Arc Welding (SMAW) performed in two high strength steels are discused. Several experimental conditions are considered in order to reproduce different environments in which hydrogen may damage the weldment perfomance. Tensile tests, microhardness, optical and scanning electron microscopy as well as scanning differential calorimetry are used to analyze hydrogen entry and its interactions with microstructure.

2. EXPERIMENTAL METHODS

In order to evaluate hydrogen incidence on welding of two high strength steels, automatic SMAW procedure was performed on a hot rolled microalloyed steel with vanadium, titanium and niobium (MLC) and on a medium carbon one (SAE 1045). The chemical composition of both steels is shown in Table 1.

Table 1. Steels chemical composition

Material	%C	%Mn	%Si	%S	%P	%Mo	%V	%Nb	%Al	%Ti	ppm N	ppm B
SAE1045	0.43	0.7	0.3	0.05	0.04	-	-	-	-	-	-	-
MLC	0.082	1.22	0.13	0.006	0.019	0.010	0.003	0.043	0.058	0.037	40	2

Considering a plate length of 150 mm for both steels, V-beveled butt-welded joint coupons with 60 ° and 30 ° angle, as specified in Figure 1, were made for the SAE 1045 and MLC steel respectively, in both cases, the filler material was a basic coated electrode (E7018), which contribute with the best mechanical properties to the welded joints.

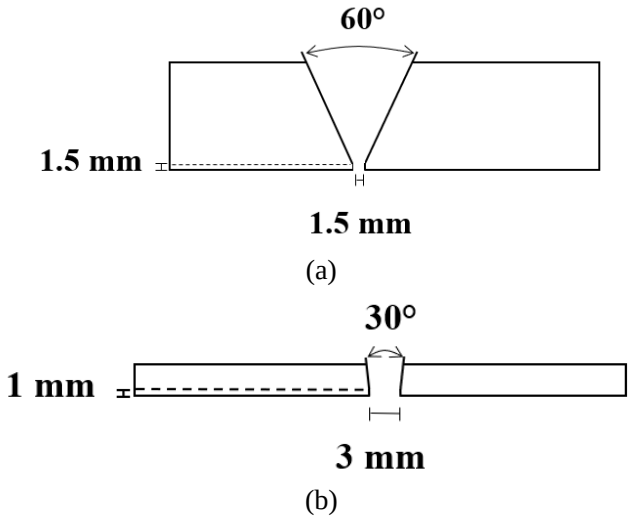

Figure 1. Steel welded coupons. (a) SAE 1045 and (b) MLC steel

Because of operational issues, two different welding coupons geometries for both materials were employed. For example, the SAE 1045 steel plate, having a larger thickness (19.05 mm) than the MLC steel (5 mm), implied that the welder needed a larger angle to weld correctly and to ensure that the heat input and its distribution was homogeneously distributed in both materials.

The diameter of the E7018 electrode was 3.2 mm for both steels. Welding parameters are detailed in Table 2. Chemical composition and main mechanical properties of filler metals are described in Table 3 and Table 4 according to standard AWS A5.1/A5.1M:2004.

Table 2. Welding parameters

Sample	Current intensity (A)	Voltage (V)	Welding torch speed (mm/s)	HI (kJ/mm)
S	127	22,2	2,8	1,24

Table 3. Chemical composition requirements for weld metal

Filler metal	%C	%Mn	%Si	%P	%S	%Ni	%Cr	%Mo	%V	Combined limit for Mn+Ni+CAR+Mo+V
E7018	0.15	1.6	0.75	0.035	0.035	0.3	0.20	0.30	0.08	1.75

Table 4. Tension test requirements for E7018 electrodes

AWS Classification	Tensile Stregth (MPa)	Yield Strength at 0.2% Offset (MPa)	Elongation Percentage in 4x Diameter Length
E7018	490	400	22

All electrodes must be dried to the right level to perform properly, even a small amount of moisture can lead to major weld problems such as internal porosity, weld cracking or poor operating characteristics. To comply with this, electrodes were submitted to a drying cycle as determined by standard AWS A5.1/A5.1M:2004, in a muffle oven preheated to 85 ºC with a heating rate of 50 ºC/h until reaching maximum temperature of 350 ºC for 1 h, Figure 2. Finally, they were slowly cooled down up to 80 ºC. Once this temperature was reached, electrodes were removed from the oven and identified as (S).

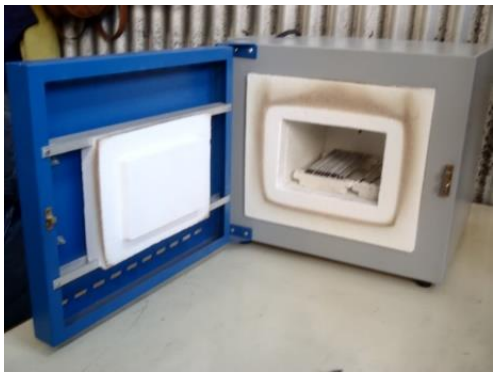

Figure 2. Drying procedure according to AWS A5.1 / A5.1M: 2004

Using these electrodes, several samples of both steels were welded. In total, 4 samples for each base metal and 2 samples for each condition, that is, samples welded with dry electrodes and with dry electrodes + H charged.

Both steels were metallurgically characterized, prior to and post welding procedures, by optical microscopy (Olympus GX51): average grain size was determined according to IRAM-IAS U 500-122 or its equivalent ASTM E112 – 13, and microhardness was measured with a 1 kg load applied for 10 seconds using a LECO model LM300AT microdurometer with a square-based pyramidal-shaped diamond indenter with face angles of 136°.

Any metallurgical analysis must begin with a detailed analysis of microstructure aspects of welded coupons. In this sense, from the microstructural point of view, the steels studied presented important differences concerning to phases distributions, as seen in Table 3.

Table 3. Microstructural composition

Material	% Ferrite	% Pearlite
MLC	86	14
SAE 1045	26	74

Microstructure in the SAE 1045 steel is mainly pearlitic with the classic lamellar morphology, Figure 3.

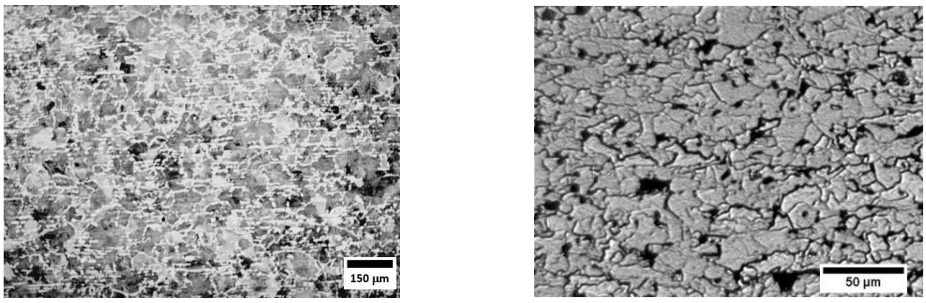

(a) (b)

Figure 3. Optical microscopy analysis of SAE 1045 steel (a) and MLC steel (b).

Inclusionary level was also analyzed and fine non-deformable oxides (diameter less than 9 µm), and fine sulfide deformable, mostly not exceeding 3 µm of thickness and 30 µm long, were found. These sulphides correspond to type II according to the Sims and Dahle (1938) classification.

The MLC steel microstructure showed to be predominantly made up of ferrite, with little presence of pearlitic lamellar microconstituent and with titanium inclusions. Average grain size in both steels showed an index of 5-6 (ASTM E112 - 13), i.e. grain size of 61.2 µm to 44.1 µm.

After welding procedure of samples, transverse flat tensile specimens were machined, as depicted in Figure 4.

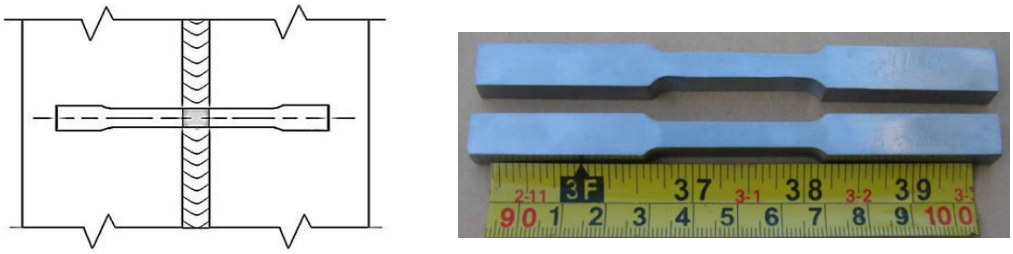

(a) (b)

Figure 4. (a) Representative scheme of flat tensile test sample extraction, transverse to the joint, (b) Samples obtained according to IRAM IAS U 500-102.

After that, a set of two samples per steel grade were electrolytically charged with hydrogen in order to simulate aggressive hydrogen input conditions. They were named SAE 1045 C and MLC C. The electrolytic hydrogen charging equipment was developed in the laboratory according to Wang et al. (2004). The cell employed consisted of 1N H_2SO_4 electrolytic solution, added with 0.25 g/L of $NaAsO_2$, hydrogen poison which inhibited its recombination reaction in aqueous solutions, thereby increasing the atomic H income into the sample, graphite anode and a constant voltage of 2.1 V for 2 h, consistent with parameters used by Marconi et al. (2014). In summary, samples welded with dry electrodes and subsequent H charged (SAE 1045 C and MLC C) and those welded only with dried electrodes without post H-charge (SAE 1045 S and MLC S), were all subjected to tensile tests in an Instron testing machine - model 1125 considering a $1.6x10^{-4}s^{-1}$ strain rate. Fracture surfaces were analyzed with a Stereo Microscope (Olympus SZ61) and a scanning electron microscope FEI Model INSPECT S50. In addition, phase percentage in base metal (BM) was quantified.

Table 4. Samples - conditions

	Samples	
Steel identification	Condition	Designation
SAE 1045	Welded with dry electrodes	SAE 1045 S
	Welded with dry electrodes + electrolitic charged of H	SAE 1045 C
MLC	Welded with dry electrodes	MLC S
	Welded with dry electrodes + electrolitic charged of H	MLC C

As a summary, Table 4 shows the working conditions of the samples used in each case. It should be noted that a set of two samples for each condition was employed for the tensile test.

Finally, differential scanning calorimetry (DSC) and silver microprint decorating techniques were employed to detect H presence and to help to understand its influence on the mechanical response of both steels.

3. RESULTS AND DISCUSSION

3.1 Welding Steel Characterization

The macrographic and micrographic analysis performed on SAE 1045 S and MLC S welded coupons revealed neither cracks nor porosity in the specimens, independent of the experimental welding conditions.

Regarding transverse microhardness measurements of welded zones, a careful procedure was considered along BM, FL and WM, for all samples welded with dry electrodes and those with H electrolytic charge.

Microhardness values across all welded samples have shown that the greatest variations are concentrated in WM-FL interfaces, with maximun microhardness peaks when crossing FL. This microhardness increase could be attributed to the fact that partially molten grains remained in the area adjacent to the liquid pool, acting as favorable nucleation sites for the new phase of the WM during solidification. In turn, the presence of martensite developments also justifies this high microhardness value.

Base metal microhardness measurements for all samples (SAE 1045 S, SAE 1045 C, MLC S and MLC C) show the same values (200 ± 2) HV, so here there is no incidence of H, however measurements in FL and WM exhibit differences whose results are shown in Figure 5. Regardless of H content, similar behavior was found in all analyzed areas for SAE 1045 steel, (Figure 5 (a)). Standard deviation of plotted measurements was ± 6 HV.

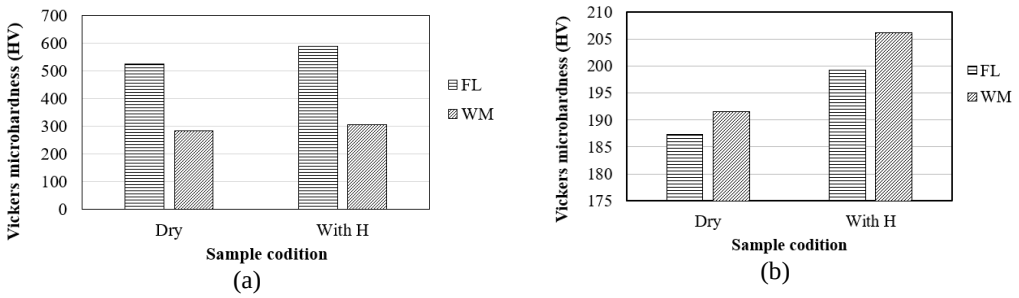

Figure 5. Vickers microhardness (HV) results, (a) SAE 1045 and (b) MLC.

In contrast, when observing Figure 5 (b), which analyzes the incidence of H on MLC steel, there are notable changes in microhardness values with respect to samples with and without H

content. The increase of microhardness in sample with H for both FL and WM is noteworthy as it could be related to H trapped in a susceptible microstructure (Srinivasan et al. 2004). The acicular microstructure presented in WM together with certain types of inclusions (strongly keen of H) would produce an increase in hardness, thus being able to generate greater susceptibility to H damage. Microhardness tests show a 10% increase in the microhardness values for the sample with H charge, compared to the uncharged one. These facts could justify the increase of the maximum mechanical strength for the H-charged sample as observed in Table 4.

Macrograph analysis depicted in Figure 6, shows the HAZ for SAE 1045 S and MLC S samples. Characteristic areas of a welded joint, that is, the weld metal (WM), the heat affected zone concerning coarse grains (HAZ CG), the heat affected zone concerning fine grain (HAZ FG) and the base metal (BM) can be clearly identified.

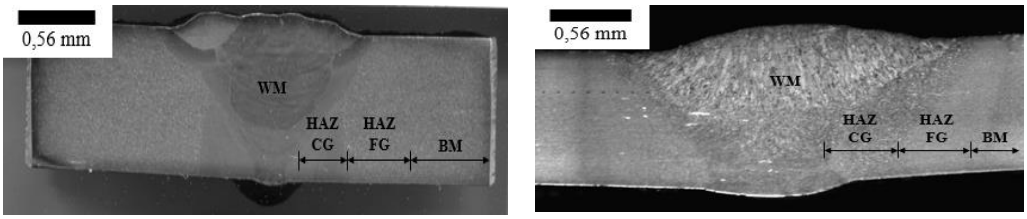

a) b)

Figure 6. Macrograph of the welded samples: a) SAE 1045 S and b) MLC S.

When analyzing the last weld bead in SAE 1045 and MLC steels, columnar structure was identified, with primary grain boundary ferrite, secondary ferrite with aligned and non-aligned second phases, and acicular ferrite, see Figures 7 and 8.

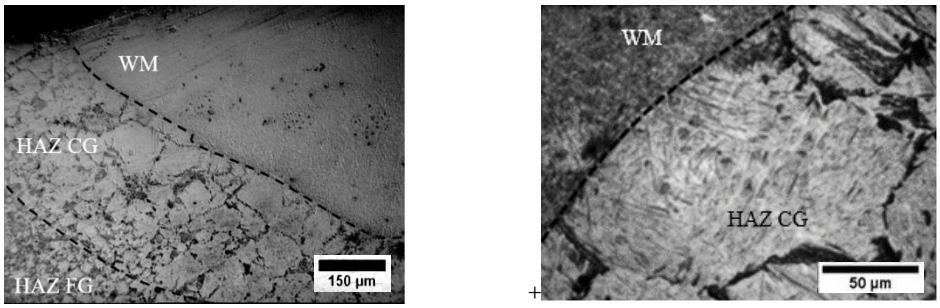

(a) (b)

Figure 7. SAE 1045 S samples, (a) Optical micrograph of the fusion zone and HAZ, and (b) Martensitic structure in HAZ CG.

It is emphasized that this last microconstituent is the most favorable, giving it greater mechanical resistance to the weld bead. Moreover, in the SAE 1045 welded coupon, the typical martensitic structure was also observed in the vicinity of the fusion line, within the HAZ CG, Figure 7 (b). The average grain size here was 170 µm. The martensite observed in the melting

zone vicinity was formed due to the prevailing high cooling rates. Both bainite and martensite provide greater dissolution capacities of H versus BM, because of the greater number of dislocations and other defects that act as traps for these interstitial atoms (Zimmer 2004).

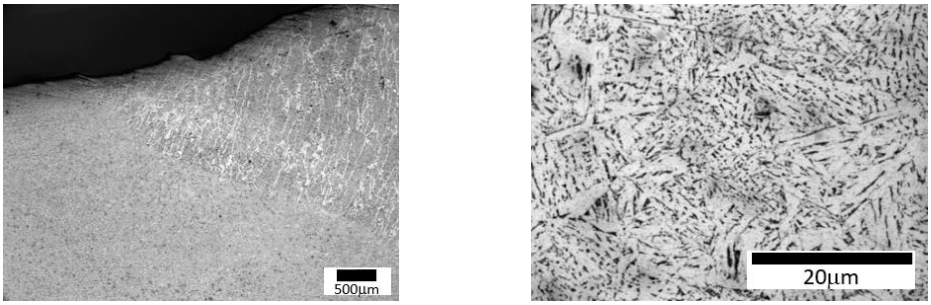

(a) (b)

Figure 8. MLC S samples, (a) Optical micrograph of the fusion zone and HAZ, and (b) Acicular structure in HAZ CG.

3.2 Tensile test results

In relation to mechanical behaviour, tensile test results (see Table 4), obtained from an average of each type of samples, were considered.

In the case of the SAE 1045 steel, it is observed that the behavior of the SAE 1045 C sample (H-charged) presented a slight increase of the ultimate tensile strength (UTS) with respect to the uncharged sample (SAE 1045 S), as expected. Possibly, H atoms were occluded in traps with low activation energy. According to the observations made by Choo and Lee (1982) and Hong and Lee (1983) for a medium carbon steel as the one used in this work, these traps could be dislocations and Feα/Fe_3C interfaces, both reversible types. It should be considered (Babu et al. 2005) that the flow of H through the material is related to the concentration gradient and the diffusivity of the material, which, in turn, would be linked to the different H entry procedures, temperature, time of exposure to the source and, obviously, to microstructure. For such a high-strength steel, the H that entered during electrolytic charge was trapped in the lattice and its interaction with the structure would be responsible for the increase in maximum resistance.

Concerning MLC steel mechanical behavior, MLC S and MLC C have broken in the WM. A slight increase in σ_Y and UTS can also be seen here for the H-charged sample (MLC C) when compared to its pair without electrolytic charge (MLC S).

Another interesting result is the strain ($\Delta\varepsilon$) reduction in all hydrogenated samples, that is, in the SAE 1045 C and MLC C samples. In these cases, hydrogen trapped in the steel lattice caused a ductility loss compared to non-charged ones (SAE 1045 S and MLC S).

Since the heat contribution during the welding process was the same in all cases, the effects on the mechanical response correspond only to H that was trapped in high energy sites. It can be inferred then, that under the conditions described, hydrogen atoms have promoted an

increment in lattice stress and, consequently, a ductility loss, in accordance with Hereñú et al. (2010) for high strength steels tested at 2.10^{-4} 1/s and with the explanation given by Aráujo et al. (2011).

Overviewing the mechanical response exhibited in Table 4, regardless of the steel grade, it follows that, H-charged samples, SAE 1045 C and MLC C, showed an increase in the σ_Y and UTS with respect to uncharged conditions (SAE 1045 S and MLC S). However, in both cases, H causes a slight decrease in elongation at maximum load, when compared to uncharged samples.

When analyzing the MLC samples fracture surface, it can be noted that all H-charged tensile specimens show a reduction in their cross section. Moreover, all samples have broken in WM region, behavior related to the presence of primary grain boundaries ferrite that have low fracture toughness and with the martensite originated in the FL area, reinforced by the H trapped in that structure.

Table 4. Mechanical properties

Sample	σ_Y *(MPa)*	*UTS (MPa)*	$\Delta\varepsilon$ *(%)*	*HV*
SAE 1045 S	466,4	661,4	18.4	529
SAE 1045 C	471,1	680,7	16.8	596
MLC S	503,4	576,4	32.4	190
MLC C	515,9	594,6	26	200

When SAE 1045 specimens fracture surface are analyzed, instead, a less rough and smoother fracture is observed in the one that was electrolytically charged with H (SAE 1045 C) when compared to the sample without hydrogen (SAE 1045 S), Figure 10(a) and 10(b). Moreover, MLC S evidences fibrous areas in the central region and an irregular breakage profile, like that presented by ductile materials, Figure 11. The sample with H content (MLC C), shows some brightness and signs of a rougher texture, has the outer edges which are smoother and straighter when compared to the MLC S specimen; aspects that would be associated with a behavior of mixed origin when tested under uniaxial tensile stress.

Observations with the scanning electron microscope (SEM) on SAE 1045 C allowed to identify localized sectors of ductility loss, Figure 10(d), with areas that look like brittle, so presenting a mixed-type fracture surface. However, it is possible to differentiate a slight increase in the dimples size in connection with Araujo et al. (2011), or Takakuwa et al. (2017), who figured out that brittle fracture could be governed by the accumulation of "ductile" fractures accompanied by localized slip deformation due to hydrogen from a microscopic point of view.

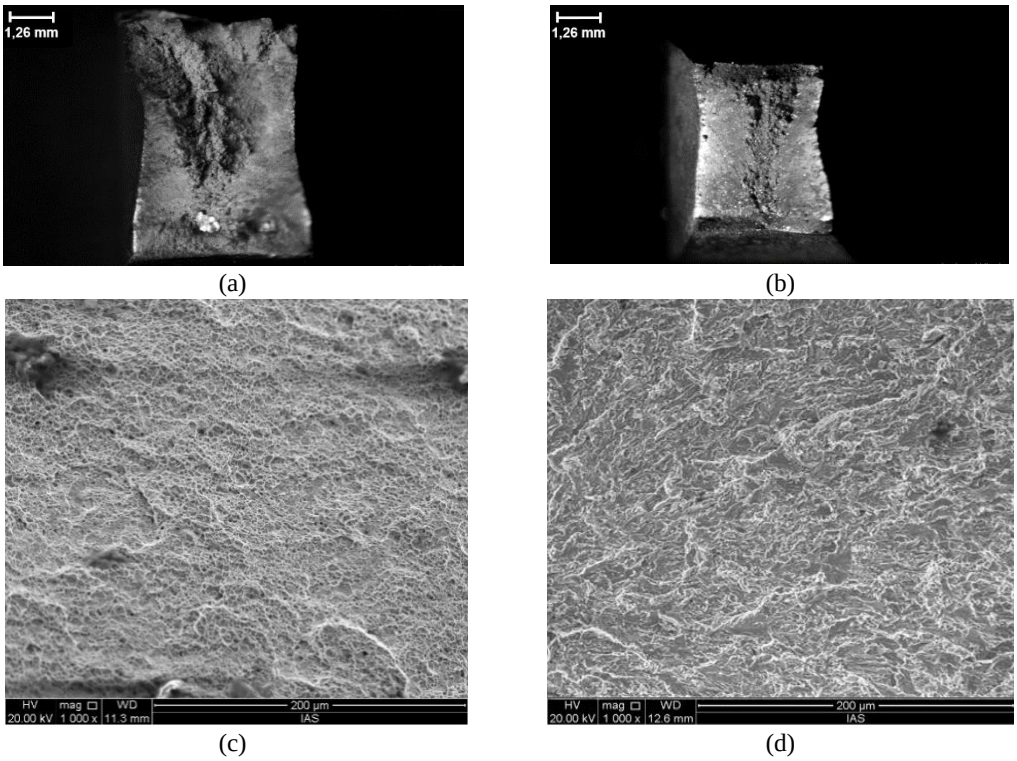

Figure 10. SAE 1045 Steel fractography with a stereoscopic magnifying glass. (a) SAE 1045 S and (b) SAE 1045 C. SEM micrographs: (c) SAE 1045 S, and (d) SAE 1045 C.

Following the guidelines outlined in previous works, (Inés and Mansilla 2012) (Inés and Mansilla 2013) studied the H embrittlement in a high strength steel through a detailed analysis of cracks and relating them to the microstructure. In this work, SAE 1045 C samples developed a small number of linear cracks, few microns in length, especially located in subsurface regions, and in no case related to inclusions. In contrast, the sample without H content (SAE 1045 S) did not show cracks in the entire section analyzed.

In the hydrogenated MLC samples, Figure 11(b), the macroscopic morphology showed that the lateral view of the fracture surface had a flat shape with sharp edges, compared to sample MLC S, Figure 11(a). Furthermore, from the microscopic point of view, MLC C samples presented the so-called quasi-cleavage morphology, thus the surface cracks and dimples areas observed, Figure 11 (c) and 11(d) looked consistent with the mechanical behavior described previously and with the lower elongation evidenced in the H-charged samples.

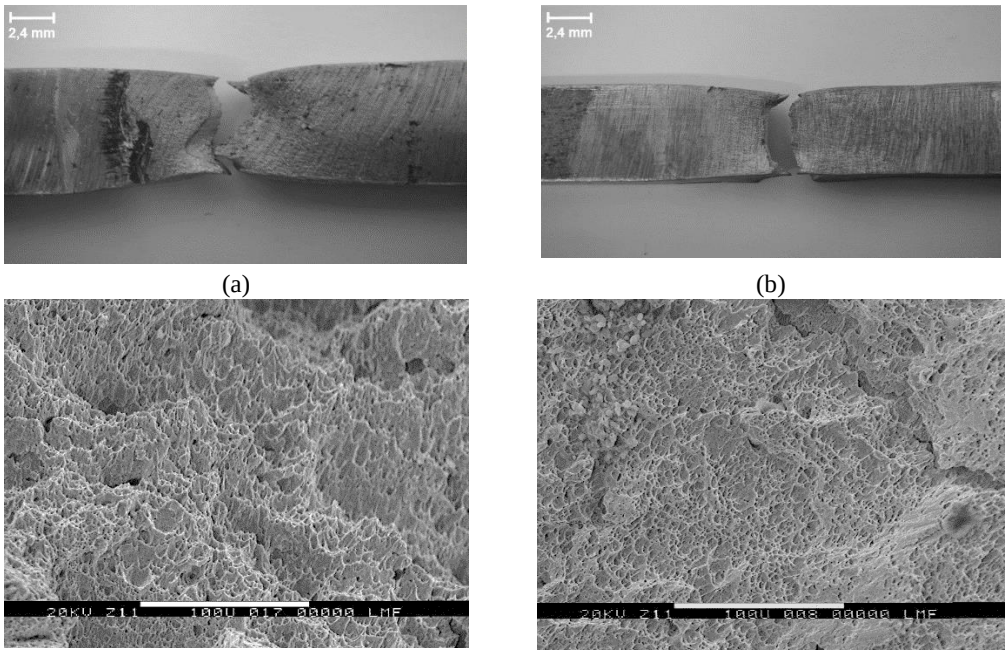

Figure 11. MLC steel fractography with stereo microscope. (a) MLC S, and (b) MLC C. SEM micrographs in: (c) MLC S, and (d) MLC C.

In order to establish the effect that H has on tensile strength of both steel grades, several formulas reported in the literature were employed, for example, (Depover et al. 2016) proposes the calculation of Hydrogen Embrittlement Index **(**HEI) using a quotient between the elongation of H charged samples during tensile tests over uncharged ones. The other method take into account equation (1), where the authors consider the HEI through the variation of the sample area of specimens with H charged and without it. This HEI can be calculated using the proposal presented by (Hazarabedian et al. 2003) in his work about hydrogen damage in soft supermartensitic stainless steel.

$$HEI = \frac{(RA_{dry} - RA_{Hcharged})}{RA_{dry}} \quad (1)$$

Table 5. Hydrogen Embrittlement Index (HEI) values

	SAE 1045	MLC	Reference
HEI	0.11	0.28	Depover et al. 2016
	0.11	0.15	Hazarabedian et al. 2003

Where $RA_{Hcharged}$ represents the percentage of the area reduction for the H charged sample, and RA_{dry} is the percentage of the area reduction for the dry one, both take as reference that of the sample untested. The HEI can vary between 0 and 1, where 0 indicates no ductility drop

and the material appears to be insensitive to hydrogen embrittlement. When an index of 1 is obtained, the ductility drop is 100% and hydrogen embrittlement is maximal. In this sense, it turned out that MLC steel had the highest index (HEI = 0.15/0.28) with respect to SAE 1045 steel (HEI= 0.11), showing the greatest sensitivity to H fracture. This was also consistent with the lowest elongation evidenced for the specimens with H charge compared to the dried ones.

Analyzing HEI results, there is a coincidence in that MLC steel is more susceptible to H embrittlement than SAE 1045 steel, aligned with the greater ductility loss manifested by this steel (see Table 4).

After the tensile tests of both steels, microhardness values in BM kept practically constant for all samples (SAE 1045 S, SAE 1045 C, MLC S and MLC C) since there was little influence of consumables. Nevertheless, martensitic developments observed in Figure 7b for the SAE 1045 steel also justify the high values obtained from microhardness. For both samples (SAE 1045 S and SAE 1045 C), the microhardness values in the FL area are higher in the H-charged samples, which would be related to H entering electrolytically. A detailed analysis of the results obtained from the tensile tests (see Table 4) together with the microhardness values observed in Figure 5, point out a low degree of H effect on mechanical behavior. That is, for sample SAE 1045 C, the results showed a slight increase in mechanical resistance values (yield stress and ultimate tensile stress) and microhardness. In turn, this sample exhibited a 4.5% reduction in elongation compared to the uncharged sample. This fact reinforces the H embrittlement effect on materials. Furthermore, this result is consistent with those presented by Candia et al. (2011) about microhardness in high strength steel and austenitic stainless steel AISI 316L. The authors state that hydrogen causes an increase in surface microhardness in electrolytically charged samples.

As mentioned previously, H in steels can be occluded at different sites, thus the knowledge of the specific traps where the H is occluded can be revealed by means of a specific metallographic technique (Shober and Dieker 1983). It is known that hydrogen absorbed in the weld pool has a propensity to diffuse within the weldment, and that high diffusivity of hydrogen in ferrite favors its rejection to HAZ adjacent to the fusion line because solubility in acicular structures is more effective in trapping H than ferrite-pearlite mixtures. Besides, apparent diffusivities are higher in martensite compared to cementite/lath interface, hydrogen is rejected from the weld metal, HAZ CG on SAE 1045 steel is trapped by the martensite developed, Figure 12. Similar results were reported (Marconi et al. 2014) regarding welding procedures in MLC steels with hydrogen charged and using the silver decoration technique. Hydrogen presence associated with complex oxides inclusion of the Ti-Mn-Si-Al type in the WM region were identified as beneficial traps for hydrogen trapping sites since they help to delay cracks developments in steels. Moreover, the increase in microhardness experienced by the WM in this MLC steel could be because of solid-solution hardening by hydrogen at static hydrogenated conditions.

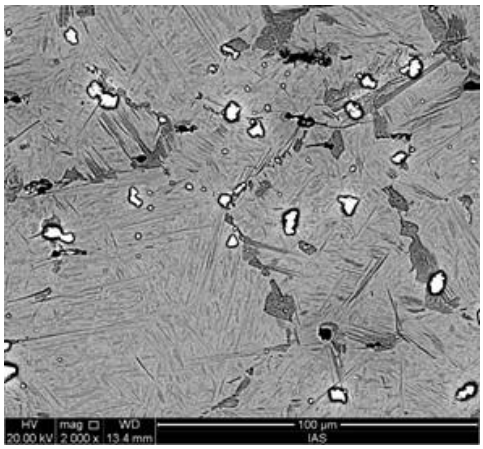

Figure 12. HAZ CG of SAE 1045, Ag particles located between Martensite needles

Hydrogen trapping behavior by inclusions was corroborated by performing DSC tests, from room temperature to 600 °C, with a heating rate of 3 °C/min. Results on MLC, Figure 13, determined that all samples analyzed (MLC S and MLC C) exhibited similar behavior at temperatures below 200°C. However, sample C showed quite higher desorption energies - absorption and desorption peaked at around 500 °C - most likely linked to the Ti inclusions present in this MLC steel, which acted as preferential H capture sites, in conformity with the available literature. As pointed out by Bhadeshia (2016) coherency of complex Ti particles determine the absorbed H within its structure and would be effective traps responsible for embrittlement. Nevertheless, when particles concentration or when coherency matrix-particles is not enough, they do not contribute to the trapping phenomenon and promote delayed fracture.

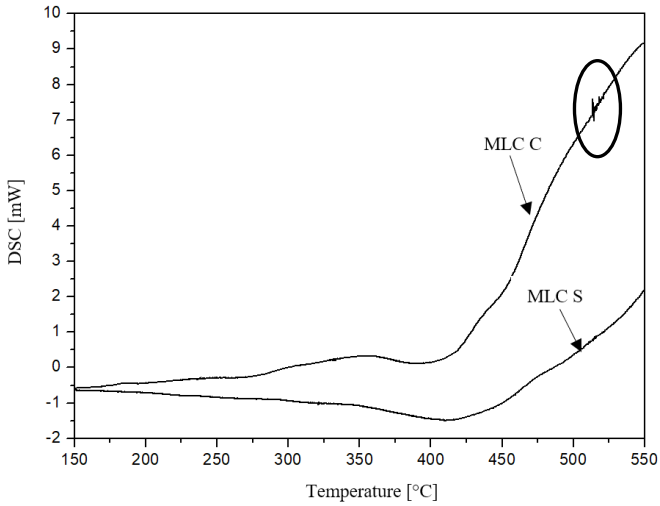

Figure 13. DSC curves for MLC steel samples.

Although some inclusions such as MnS in SAE 1045 are associated with large H trapping energies, harmful effect depends mainly on size and distribution. On the other hand, for MLC

samples, Figure 14, some white particles were detected (Ag particles), related to Ferrite-complex Ti-Mn-Si-Al oxides interfaces, indicated by EDS analysis. This result verifies the close relationship of the H income during welding with silver particles, mainly related to inclusions.

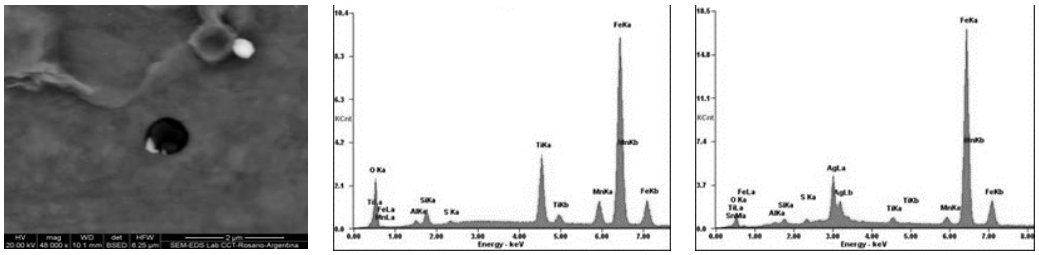

(a) (b) (c)

Figure 14. (a) TiO_2 inclusion (dark) with silver particle (white), (b) and (c) EDS of inclusion and white particle shown in a).

Consequent with all experimental evidence collected in this work, the observed mixed fractures acompanied by "brittle zones" may be associated with H anchored at inclusions and martensite needles, promoting localized slip deformation from a microscopic point of view and consequent with HELP embrittlement mechanism.

Although mixed mode fracture because of H indicate some degree of influence on mechanical properties, low HEI indexes calculated enable the application of both steels in high hydrogen environments because traps are not harmful under the analized conditions.

CONCLUSION

As regards mecanical behaviour, an explanation about H incidence on these steels, welded by SMAW process, may be outlined as follows:

For all H-charged samples, SAE 1045 C and MLC C, an increase in tensile strength and a ductility loss at maximum load was evidenced, when compared with uncharged ones. This behavior is more noticeable in MLC steel, because of titanium inclusions constitute the main H trapping sites. Moreover, this behavior is coincident with the so-called quasi-cleavage morphology of the fracture surface after tensile test and with the highest microhardness difference. However, in SAE 1045, martensite needles are responsible for H capture, carring – for this steel grade – low hydrogen embrittlement index. Therefore, H trapped during electrolytic charges and then occluded in fusion line and weld metal areas justify the mechanical properties variations of these steels.

It can be concluded that, although both steels are not susceptible to the hydrogen embrittlement phenomenon, under the experimental conditions imposed here, the MLC proved to be the most sensitive steel. In consequence, relevant care on welding must be taken into account to prevent the mechanical properties impoverishment and consequent embrittlement during later processes to prevent delayed fracture.

REFERENCES

Antoniolli, I., Guariente, P., Pereira, T., Pinto Ferreira, L., and Silva, F. J. G.. 2017. "Standardization and Optimization of an Automotive components production line." *Procedia Manufacturing* 13, 1120-1127. doi: 10.1016/j.promfg.2017.09.173.

Alam, N., Li, H., Chen, L., and Dunne, D. 1997. "Effect of hydrogen on fracture morphology of hydrogen assisted cracking in steel weldments". Paper presented at the International Conference on Frature, Sydney, Australia, April 1-5.

Araújo, B.A., Palma, J.A., Vilar, E.O. and Silva, A.A. 2011. "Hydrogen embrittlement of API 5l x60 and API5l x80 Steels", *Revista Información Tecnológica*, 129-140, 22, 6.

Babu, S., Feng, Z., Santella, M.L., David, S.A, Lencoe, J.G,. Anovitz, L. and Korinko, P.S. 2005. "Hydrogen permeability and Integrity of hydrogen transfer pipelines", *Hydrogen Pipeline R&D, Project Review Meeting Oak Ridge National Laboratory*, Oak Ridge, United States.

Banerjee, A., Debroy, T., Onneby, C. and Small, M. 1993. "Recent trends in welding science and technology", *ASM International*, 39.

Bertolino, G. 2012. Deterioro de las propiedades mecánicas de aleaciones base circonio por interacción con hidrógeno [Mechanical properties deterioration of the of zirconium-based alloys due to hydrogen interaction] (in Spanish), PhD diss, Instituto Balseiro, Comisión de Energía Atómica, Universidad Nacional de Cuyo, Argentina.

Bhadeshia, H. K. D. H. 2016. "Prevention of Hydrogen Embrittlement in Steels". *ISIJ International*, 56: 1, 24–36.

Candia, Graciela L., Brandaleze, Elena, and Mansilla, Graciela A. 2011. "Estudio del efecto del hidrógeno sobre la microdureza de aceros [Study of the effect of hydrogen on the microhardness of steels] (in Spanish)". Paper presented at the annual metting HYFUSEN 2011, Mar del Plata, June 6 - 11.

Choo, W.Y.and Lee, J.Y. 1982. "Hydrogen trapping phenomena in carbon steel". *J Mater Sci 17*, 1930–1938. doi:10.1007/BF00540409

Coudreuse, L. and Charles, J. 1987. "The use of a permeation technique to predict critical concentration of H2 for cracking". *Corrosion Science* 27, 10/11: 1169-1181.

Ćwiek, J. 2005. "Hydrogen assisted cracking of high-strength weldable steels in sea-water". *Journal of Materials Processing Technology*, 164-165: 1007-1013.

Davidson, J.L. 1998. *Australian Welding Journal* 43:33-39.

Davis, J.R. 2006. Corrosion of Weldments, Davis & Associates. *ASM International, Materials Park, OH* 44073-0002, 24-26.

Djukic M. B., Bakic G. M., Zeravcic V. S., Sedmak A., Rajicic B. 2019. "The synergistic action and interplay of hydrogen embrittlement mechanisms in steels and iron: Localized plasticity and decohesion". *Engineering Fracture Mechanics 216*. Doi: 2019.106528.

Echegoyen, R., Zappa, S., Svoboda, H.G., Surian, E.S. and De Vedia, L.A. 2009. "Daño por hidrógeno en depósitos de soldadura de acero inoxidable supermartensítico [Hydrogen damage in supermartensitic stainless steel welding tanks] (In Spanish)", Paper presented at the annual Congreso SAM/CONAMET, Buenos Aires, Argentina, November 22-25.

Frappart, S., Oudriss, A., Feaugas, X., Creus, J., Bouhattate, J., Thébault, F., Delattre, L. and Marchbois, H. 2011. *Scr. Mater.*, 65, 859.

Fydrych, Dariusz and Rogalski, Grzegorz. 2013. "Weldability of high strength steels in wet welding conditions". *Polish Maritime Research* 20, 67-73. doi: 10.2478/pomr-2013-0018.

Gedeon, S.A. and Eagar, T.W. 1990. *Weld. J. Res. Suppl.,* 69, (7), 264.

Hazarabedian, A., Bilmes, P., Llorente, C. and Ovejero García J. 2003. "Efecto de los tratamientos térmicos de post soldadura sobre la resistencia al daño por hidrógeno de aceros inoxidables soft martensíticos [Effect of post-weld heat treatments on hydrogen damage resistance of soft martensitic stainless steels] (*in Spanish*)". Paper presented at 12nd SAM/CONAMET, San Carlos de Bariloche, Argentina, November 17-21.

Hereñú, S., Armas, Alberto., Brandaleze, Elena and Mansilla, Graciela A. 2010. "Hydrogen influence on the mechanical behaviour of high strength steel", *MP MaterialsTesting,* 610-614, 52, 9.

Hirth, J. P. 1980. *Metall. Transactions A,* 11 A(6), 861-889.

Hong, J.Y. and Lee, G.W. 1983. *J Mater 18,* 271-277.

Inés, Mariano N., Asmus, Carolina and Mansilla, Graciela A. 2013. "Influencia del grado de deformación sobre la fragilización por hidrógeno en un acero de alta resistencia [Influence of the degree of deformation on hydrogen embrittlement in a high strength steel] (in Spanish)". Paper presented at 13° Congreso Internacional en Ciencia y Tecnología de Metalurgia y Materiales, Puerto Iguazú, Argentina, August 20-23.

Inés, Mariano N., Mansilla and Graciela A. 2013. "Effect of hydrogen concentration and MnS inclusions on the embrittlement of a high strength steel". *Acta Microscopica 22*, 1, 20-25, ISSN 0798-4545.

Inés, Mariano N. and Mansilla, Graciela A. 2012. "Trampas irreversibles, su influencia en la fragilizacion de un acero de alta resistencia. [Irreversible traps, their influence on the embrittlement of a high strength steel] (In Spanish)". Paper presented at 12º Congreso Binacional de Metalurgia y Materiales, Chile, October 22-26.

Katano, G., Ueyama, K. and Mori, M. 2001. *J. Mater. Sci*., 36, 2277.

Kim, J., Lee, Y., Park, K. and Lee, C. 2009. *Materials Science and Engineering A,* 505, 105110.

Kumar, P. G. and Yu-ichi, K. 2013. "Diffusible hydrogen in steel weldments". *Trans. JWRI 42*, 39-62.

Linnert, G.E. 1965. *Welding Metallurgy, Carbon and Alloy Steels: Fundamentals, 1,* AWS.

Marconi, Cesar, Sabusechi, Damaris, Asmus Carolina, Mansilla, Graciela A. 2014. "Efecto del hidrógeno atrapado en junta soldada de acero microaleado de alta resistencia. [Effect of hydrogen trapped in welded joint of high strength microalloyed steel] (in Spanish)". Paper presented at 3rd National Meeting of Technological Materials in Argentina - Matte@r 2014, National Technological University, La Plata, May 13-15.

Marconi, Cesar, Sabusechi, Damaris, Asmus, Carolina and Mansilla, Graciela A. 2014. "Análisis de la degradación por hidrógeno en uniones soldadas de acero microaleado. [Analysis of hydrogen degradation in welded joints of microalloyed steel] (in Spanish)". Paper presented at Congreso Internacional de Metalurgia y Materiales Sam-Conamet/Iberomat/Materia, Santa Fe, Argentina, October 21–24.

Maroef, I., Olson, D. L., Eberhart, M. and Edwards, G. R. 2002. *Int. Mater. Rev.*, 47, 191.

Mundra, K., Blackburn, J. M., DebRoy, T. 1997. "Absorption and transport of hydrogen during gas metal arc welding of low alloy steel". *Science and Technology of Welding and Joining,* 2-4.

Nagumo, M. 2001. *ISIJ International 41,* 6, 590-598.

Nelson, H.G. 1974. "Testing for Hydrogen Environment Embrittlement: Primary and Secondary Influences". *ASTM STP 543, American Society of Testing and Materials*, 152-169.

Nordlander, P., Norskov, J. K and Besenbacher F. 1986. *J. Phys. F: Metal Phys.*, 16, 1161.

Novak, P., Yuan, R., Sofronis, P. and Ritchie, R. O. 2010. *Journal of the Mechanics and Physics of Solids*, 58, 206-226.

Ouden, G. and Griebling, O. 1990. "Recent trends in welding science and technology". *ASM International 431*.

Padhy, G. K. And Komizo, Y. 2013. "Diffusible Hydrogen in Steel Weldments- A Status Review". *Transactions of JWRI*, 42, 1.

Pal, V. K., Singh, L. P. And Pandey, C. 2017. "Control of Hydrogen assisted cracking in High Strength Steel Welds". *International Journal of Engineering Sciences & Research Technology*, ISSN: 2277-9655 - 6(4).

Pandey, C., Mahapatra, M. M., Kumar, P., and Saini, N. 2017. *J. Eng. Mater. Technol.*

Pandey, C., Saini, N., Mahapatra, M. M., and Kumar, P. 2016. *Int. J. Hydrogen Energy.*

Pitrun, M. 2004. "The effect of welding parameters on levels of diffusible hydrogen in weld metal deposited using gas shielding rutile rlux cored wires". PhD diss, The University of Wollongong, Dpt. of Materials Engineering.

Rudomilova, D., Prošek, T. and Luckeneder, G. 2018. "Techniques for investigation of hydrogen embrittlement of advanced high strength steels". *Corros Rev*; 36(5): 413–434.

Shober, T., and Dieker, C. 1983. "Observation of Local Hydrogen on Nickel Surfaces." *Metallurgical Transactions A,* 14 (11):2440-2442.

Sims, C. E., and Dahle, F. B. 1938. *Trans. Am. Foundarymen'sAss* 46:65.

Singh, S.K. and Sasmal, S. 2004. "Effect of hydrogen on toughening of a low alloy steel", *ISIJ International*, 44:1, 203-208,. Doi:10.2355/isijinternational.44.203

Srinivasan, P. B., Sharkawy, S.W. and Dietzel, W. 2004. "Environmental cracking behavior ofsubmerged arc-welded supermartensitic stainless steel weldments", *Journal of Materials Engimeering and Performance*, 13 (2), 232 - 236.

Stratmann, M. 2003. *Encyclopedia of Electrochemistry Corrosion and oxide films*, Vol. 4, 108-145

Suh, D. W. 2014. *Mater. Sci. Technol.*, 30, 1131.

Takakuwa, O., Yamabe, J., Matsunaga, H., Furuya, Y., Matsuoka, S. 2017. "Comprehensive understanding of ductility loss in various steels with external and internal hydrogen". *Metallurgucal an materials transactions A 48*, 5717–5732. doi:10.1007/s11661-017-4323-3

Tasak, E. 2002. *Weldability of steel.* Wydawnictwo Fotobit (Fotobit Publishers), Cracow.

Wang, T. Y., Kanedome, M., Yasuda, T., Suda, T., Watanabe, S., Ohnuki, Nagasaka, T., and Muroga, T. 2004. "Dynamic and static hydrogen charging effects on mechanical properties in pure Vanadium". *Journal of Nuclear Materials*, 329-333 (A):477-480.

Wasim, M. and Djukic, M. 2019. "Hydrogen embrittlement of low carbon structural steel at macro-, micro- and nano-levels". *International Journal of Hydrogen Energy*. DOI: 10.1016/j.ijhydene.2019.11.070.

Wildash, C., Cochrane, R.C., Gee, R. and Widgery, D.J. 1998. *Proceedings of the 5th International Conference on Trends in Welding Research. Pine Mountain*. 1-5 June, 745-750.

Yue, X. 2014. *Weld. World 59*, 77.

Zafra, A., Peral, L.B., Belzunce, F. and Rodríguez, C. 2018. "Effect of hydrogen on the tensile properties of 42CrMo$_4$ steel quenched and tempered at different temperatures". *International Journal of Hydrogen Energy 43*. DOI: 10.1016/j.ijhydene.2018.03.158.

Zimmer Peter Kannengiesser, B. T. 2004. "Effects of hydrogen on weld microstructure mechanical properties of the high strength stells S690Q and S1100QL". *Federal Institute of Materials Research and Testing (BAM)* Unter den Eichen 87 D-12200 Berlin, Germany.

Depover T., Wallaert, E., Verbeken, K. 2016. "Fractographic analysis of the role of hydrogen diffusion on the hydrogen embrittlement susceptibility of DP steel". *Materials Science&EngineeringA* 649, 201–208